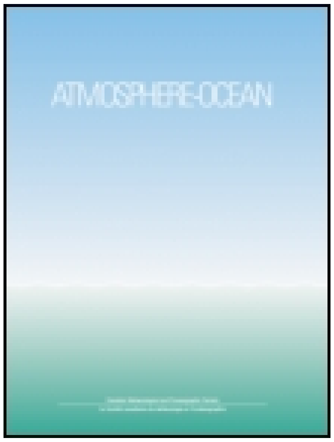

Atmosphere-Ocean

Publication details, including instructions for authors and subscription information:
http://www.tandfonline.com/loi/tato20

Glacial ocean circulation and property changes in the North Pacific

Seong-Joong Kim [a] & Young-Gyu Park [b]

[a] Korea Polar Research Institute , KORDI , Songdo Techno Park, Incheon, 406-840, Korea E-mail:

[b] Korea Ocean Research and Development Institute , P.O. Box 29, Ansan, 425-600, Korea

Published online: 21 Nov 2010.

Glacial Ocean Circulation and Property Changes in the North Pacific

Seong-Joong Kim[1,*] and Young-Gyu Park[2]

[1]*Korea Polar Research Institute, KORDI*
Songdo Techno Park, Incheon 406-840, Korea
[2]*Korea Ocean Research and Development Institute*
P.O. Box 29, Ansan 425-600, Korea

[Original manuscript received 11 April 2007; accepted 6 October 2007]

ABSTRACT *The glacial water properties and circulation changes in the North Pacific Ocean are investigated using a coupled ocean-atmosphere-sea-ice climate model. With glacial boundary conditions, an increase in potential density in the upper layers of the northern North Pacific makes the water column highly unstable and eventually results in the enhancement of North Pacific Intermediate Water (NPIW) production, consistent with proxy evidence. The NPIW outflow reaches deeper layers than in the present-day ocean, but remains largely confined to the North Pacific. The increase in potential density is predominantly caused by the increase in salinity and, to a lesser extent, by decreases in temperature. The increase in surface salinity is especially high in the Sea of Okhotsk and the western Bering Sea, which are possible source areas of glacial NPIW production. In these regions, an increase in brine release due to a marked increase in sea ice, evaporation exceeding precipitation, and a reduction in river discharge contribute to the increase in surface salinity. In short a reduction in freshwater input to the northern North Pacific is the main reason for the increase in the production and outflow of glacial NPIW.*

RÉSUMÉ *[Traduit par la rédaction] Nous étudions les changements dans les propriétés et la circulation glaciaire dans l'océan Pacifique Nord au moyen d'un modèle climatique couplé océan-atmosphère-glaces de mer. Avec des conditions glaciaires aux limites, une augmentation de la densité potentielle dans les couches supérieures du Pacifique Nord septentrional rend la colonne d'eau très instable et entraîne éventuellement une accélération de la production d'eaux intermédiaires du Pacifique Nord, qui s'accorde avec les preuves indirectes. La sortie d'eaux intermédiaires du Pacifique Nord atteint des couches plus profondes que dans l'océan actuel mais demeure largement confinée au Pacifique Nord. L'accroissement de densité potentielle est principalement causé par l'accroissement de la salinité et, dans une moindre mesure, par des diminutions de température. L'accroissement de la salinité en surface est particulièrement marqué dans la mer d'Okhotsk et dans l'ouest de la mer de Béring, qui sont des régions sources possibles de production d'eaux intermédiaires du Pacifique Nord glaciaires. Dans ces régions, une augmentation du rejet de saumure causé par une augmentation marquée des glaces de mer, l'excès de l'évaporation sur les précipitations et une réduction des débits fluviaux contribuent à l'accroissement de la salinité en surface. En résumé, la réduction de l'apport d'eau douce dans le Pacifique Nord septentrional est la principale raison de l'accroissement dans la production et la sortie d'eaux intermédiaires du Pacifique Nord glaciaires.*

1 Introduction

The circulation and properties of the oceans play a critical role in regulating the Earth's climate, such as moderating heat and freshwater balances and influencing atmospheric CO_2 concentration (Broecker, 1997). Understanding the glacial/interglacial variations in the deep ocean is thus critical in assessing and predicting future climate change.

In the present-day ocean, the deep water is largely comprised of two distinct water masses: relatively warm and saline North Atlantic Deep Water (NADW) and relatively cold and fresh Antarctic Bottom Water (AABW) (Warren, 1981; Killworth, 1983). Unlike the North Atlantic and Antarctica, deep convection does not occur in the North Pacific because the surface water in the northern North Pacific is too fresh with annual mean salinities of approximately 32.7 psu which is much lower than the underlying deep water salinities of 34.6–34.7 psu even when the surface water freezes (Warren, 1983). In the northern North Atlantic, on the other hand, the average surface salinity is 34.9 psu and is much closer to the deep water salinities (34.9–35.0 psu). Therefore, the northern North Atlantic is less stably stratified

*Corresponding author's e-mail: seongjkim@kopri.re.kr

so that deep convection could be induced by a weak buoyancy loss, in contrast to the northern North Pacific.

Above the deep waters, relatively fresh intermediate waters are found in both the North Atlantic and the North Pacific. The intermediate waters are composed of Labrador Sea Water (Talley and McCartney, 1982) and Antarctic Intermediate Water (AAIW) (McCartney, 1977; Molinelli, 1978; Schmid et al., 2000; Sørensen et al., 2001) in the North Atlantic, and North Pacific Intermediate Water (NPIW) (Talley, 1985, 1993) in the North Pacific. NPIW is characterized by a well-defined salinity minimum at 500–700 m with a relatively narrow density range from 26.7 to 26.9 kg m^{-3} (Svedrup et al., 1942; Reid, 1965; Talley, 1985, 1993, 1997; Yuan and Talley, 1996; Yasuda, 1997; Freeland et al., 1998; Watanabe and Wakatsuchi, 1998; Kobayashi, 1999; Shcherbina et al., 2003). Even though NPIW is widely distributed at depths of 300–800 m in the North Pacific, it is not yet clearly understood where and how it is produced. The preponderance of recent observations suggests that NPIW might be produced in the Sea of Okhotsk by wintertime brine rejection (Kitani, 1973; Talley, 1991, 1993; Yasuda, 1997; Freeland et al., 1998; Gladyshev et al., 2000; Shcherbina et al., 2003). The Sea of Okhotsk provides favourable conditions for initial dense water formation by high ice production in the northwestern polynya combined with cyclonic circulation (Shcherbina et al., 2003). The production rate of NPIW is suggested to be about 2 Sv (1 Sv = 1 × 10^6 m^3 s^{-1}) (Macdonald, 1998; Talley, 2003).

Some geological and geochemical evidence suggests that during the last glacial period the ocean circulation in the North Pacific differed from present-day conditions. For example, by using δ^{13}C measured in benthic foraminifera as a water mass tracer, Oppo and Fairbanks (1987) showed that the water mass from the Southern Ocean was dominant in the North Pacific, with little NADW contribution during glacial periods. Curry et al. (1988) and Duplessy et al. (1988) reported the δ^{13}C distribution in the world ocean from benthic foraminifera and obtained a glacial δ^{13}C concentration in the North Pacific that is lower than at present and is as low as that of the Southern Ocean. By measuring glacial nutrient content using Cd/Ca content, Boyle (1992) concluded that the Cd content of the glacial deep waters of the northwest Pacific was 20–30% lower than that of the present-day ocean. These two results indicate a new source of nutrient-depleted water in the North Pacific. Okouchi et al. (1994) compared the Cd concentration in bottom sediment cores sampled in the northwestern Pacific off Japan at depths of approximately 2700 m with those sampled in the western equatorial Pacific off New Guinea (160°E). In the northwestern Pacific, the Cd concentration is about 20% lower during the last glacial period than it was during the Holocene, whereas in the western equatorial Pacific it increases slightly. They suggested that there was a convection cell in the North Pacific that was not strong enough to expand to equatorial regions where the nutrient-rich water originating in the Southern Ocean is found. From stable isotopes and geochemical evidence, Gorbarenko (1996) suggested that there was a possible intensification of intermediate water formation in the northwestern Pacific including the Okhotsk and Bering seas during the glacial period. By synthesizing sediment cores of benthic foraminiferal δ^{13}C and δ^{18}O in the North Pacific, Keigwin (1998) concluded that during the glacial period there were better ventilated and fresher water masses at intermediate depths, but deep water was as nutrient-rich as today, in contrast to previous estimates. Even though there is some disagreement regarding the glacial deep water status, the majority view is that the production of the glacial intermediate or upper deep water shallower than about 2500 m was enhanced in the North Pacific.

Boyle (1997) summarized the glacial intermediate/deep ocean circulation based on both δ^{13}C and Cd/Ca estimates of benthic foraminifera (see Fig. 1 in Boyle (1997)). He divided major flows into upper deep (about 1.5–2.5 km) and lower deep (2.5–5 km) sections. In the glacial period, NADW shifted to shallow depths and recirculated to the north at the tip of Africa into the Indian Ocean without fully reaching the Southern Ocean. AABW appears to flow more extensively to the north in all ocean basins including the North Pacific. Although highly uncertain, it is suggested that there are possible sources of intermediate/deep water in the Sea of Okhotsk and the Bering Sea as there was in the glacial North Atlantic.

Geological and geochemical proxy data have provided useful information for glacial ocean conditions, but these data are limited in their ability to reveal how the ocean conditions were determined. As a complement to proxy studies, a hierarchy of physically based numerical models has been used to study the mechanisms associated with glacial climate change. Fully coupled models (i.e., models that include three-dimensional representations of atmospheric and oceanic general circulation, including sea-ice physics) represent relatively comprehensive and physically based tools for simulating past ocean changes. Several fully coupled model glacial simulations have been reported (e.g., Bush and Philander, 1999; Hewitt et al., 2001; Kitoh et al., 2001; Shin et al., 2003; Kim et al., 2002, 2003; Kim, 2004a, 2004b; Peltier and Solheim, 2004; Kageyama et al., 2006; Yanase and Abe-Ouchi, 2007), but to our knowledge detailed analyses of glacial ocean circulation and property changes in the North Pacific have not yet been made. In this study, the ocean circulation and property changes of the intermediate or deep water masses in the North Pacific during the glacial period are examined using a coupled model.

2 Numerical model and experimental design

The model employed in the current study is the second generation Canadian Centre for Climate Modelling and Analysis (CCCma) coupled general circulation model. The atmospheric component of the coupled model is a primitive equation model characterized by T32 horizontal resolution corresponding to a 3.75° Gaussian grid, and 10 vertical levels (McFarlane et al., 1992). Cloud formation is parameterized through relative humidity and the surface albedo is evaluated depending on the surface type. A simple river routing scheme is included to represent the freshwater flux to the ocean. The oceanic component is a modified from the Geophysical Fluid Dynamics Laboratory Modular Ocean Model (GFDL MOM) version 1.1 (Pacanowski et al., 1993). The horizontal and vertical resolutions are 1.875° × 1.875° and 29 vertical layers. Ocean mixing is represented by vertical and isopycnal diffusion along with the eddy-induced mixing parameterization of Gent and McWilliams (1990). The isopycnal diffusivity is 1000 $m^2 s^{-1}$ with a background horizontal diffusivity of 100 $m^2 s^{-1}$. Vertical diffusivity is 3×10^{-5} $m^2 s^{-1}$. When the density stratification is unstable, convective adjustment is performed by increasing the vertical diffusivity. The coupled model includes a representation of sea-ice thermodynamics from Semtner (1976) and sea-ice dynamics from Flato and Hibler (1992). A more detailed description of the atmosphere, ocean, sea-ice, and land surface components of the coupled model is given in other papers (Flato and Boer, 2001; Kim et al., 2002, 2003, and references therein).

The atmospheric and oceanic components interact once per day exchanging heat, fresh water, and momentum. A fixed annual cycle of heat and freshwater flux adjustment fields computed from a preliminary run of the coupled model are applied over both ice-covered and open ocean and do not change as the climate evolves. The flux adjustment has been applied in some climate modelling and is used to account for biases in various components that would otherwise cause the model to exhibit a secular drift in its control climate. All experiments are undertaken as perturbations about this control climate. To avoid any artificial feedbacks associated with these flux adjustments, they are applied in the control and glacial experiments in exactly the same way and do not vary with time and space. Boer et al. (2000a, 2000b) and Flato and Boer (2001) applied similar flux adjustments to those used in this study in their climate simulations for the twentieth and twenty-first centuries and obtained a reasonable degree of future climate change, including regions of sea-ice change, in comparison to other non-flux corrected simulations. This indicates that flux adjustment fields obtained from present conditions hold true under different climate scenarios.

Two simulations are analyzed in this study. The control simulation has a specified CO_2 concentration of 330 ppm and a contemporary land mask and topography. The glacial simulation features a decreased CO_2 concentration of 235 ppm, a value chosen to reproduce the greenhouse gas forcing difference between pre-industrial (280 ppm) and glacial maximum conditions (200 ppm from Petit et al. (1999)), and ice sheet topography using the ICE-4G reconstruction at 21,000 years before present from Peltier (1994). The ice sheet volume requires an estimated glacial sea level drop of 120 m (Fairbanks, 1989; Yokoyama et al., 2000; Clark et al., 2001). This is equivalent to about 3% of the total ocean volume and results in an increased global mean salinity of about 1 psu (Broecker, 1982). In the glacial simulation, the land mask is modified to match the sea level change, but for convenience the ocean volume (thus the global salinity) is not modified. Because the salinity increased homogeneously throughout the entire glacial ocean by long-term diffusion as reported in Boyle (2002), it may not influence global ocean dynamics. Orbital parameters and vegetation and soil types are unchanged. During the last glacial maximum (approximately 21,000 years before present) the periods of obliquity (41,000 years) and precession (23,000 and 19,000 years) are almost the same as at present and the eccentricity (with a period of 100,000 years) is also basically unchanged. Therefore, the annual-mean radiative forcing change induced by glacial orbital parameters is indeed negligible as shown by several model studies (e.g., Hewitt and Mitchell, 1997; Broccoli, 2000). Although the effect of vegetation on the glacial climate may not be negligible on a regional basis, the global impact is of less importance (Crowley and Baum, 1997; Wyputta and McAvaney, 2001). To save computing effort, the ocean component is accelerated in the glacial simulation using a periodically synchronous coupling method (for more details see Kim et al. (2003)).

3 Results and discussion

In order to check how the model reproduces the present-day climate, observed salinity and temperature are compared with the control simulation. Figure 1 compares the zonally and meridionally averaged annual-mean sections of observed salinity with the salinity from the control simulation in the North Pacific. The most distinctive feature of the observations is the southward extension of a fresh tongue of salinity less than 34.5 psu at a depth of about 500–700 m. This salinity minimum tongue is the NPIW outflow reported in many earlier studies (Svedrup et al., 1942; Reid, 1965; Talley et al., 1995; Talley, 1997; Yasuda et al., 1996; Yasuda, 1997; Kobayashi, 1999). In the meridional section, the outcrop of the 33.8 psu isohaline marks the southern boundary of the subarctic front, while the outcrop of the 33.0 psu isohaline defines the northern boundary of the frontal zone (Yuan and Talley, 1996). Although the location of the front varies with time and space, the subarctic front is usually found between 40°–45°N and accompanies the North Pacific current. The shallow salinity minimum layer is found north of the front. The shallow salinity maximum layer is observed at about 25°N and relatively saline water originating from the Southern Ocean is found below the NPIW tongue.

The features found in the observed sections are reproduced reasonably well in the control simulation as displayed in Figs 1b and 1d. First, the propagation of the fresh NPIW outflow tongue to the south is clearly reproduced. Second, the subarctic front is represented between 35°–45°N, slightly south of the observed location. Third, the relatively saline subtropical water to the south of the front and the salinity minimum to the north of the front are well simulated. Finally, in the zonal section the simulated salinity minimum layer resembles that of the observed layer. The salinity of the simulated NPIW tongue is slightly higher than observed. The saltier property of the simulated NPIW seems to be due to both the slightly more saline surface water in the northern North Pacific and the more saline deep water below.

Figure 2 displays the observed and simulated zonal- and meridional-mean potential temperatures, respectively. The

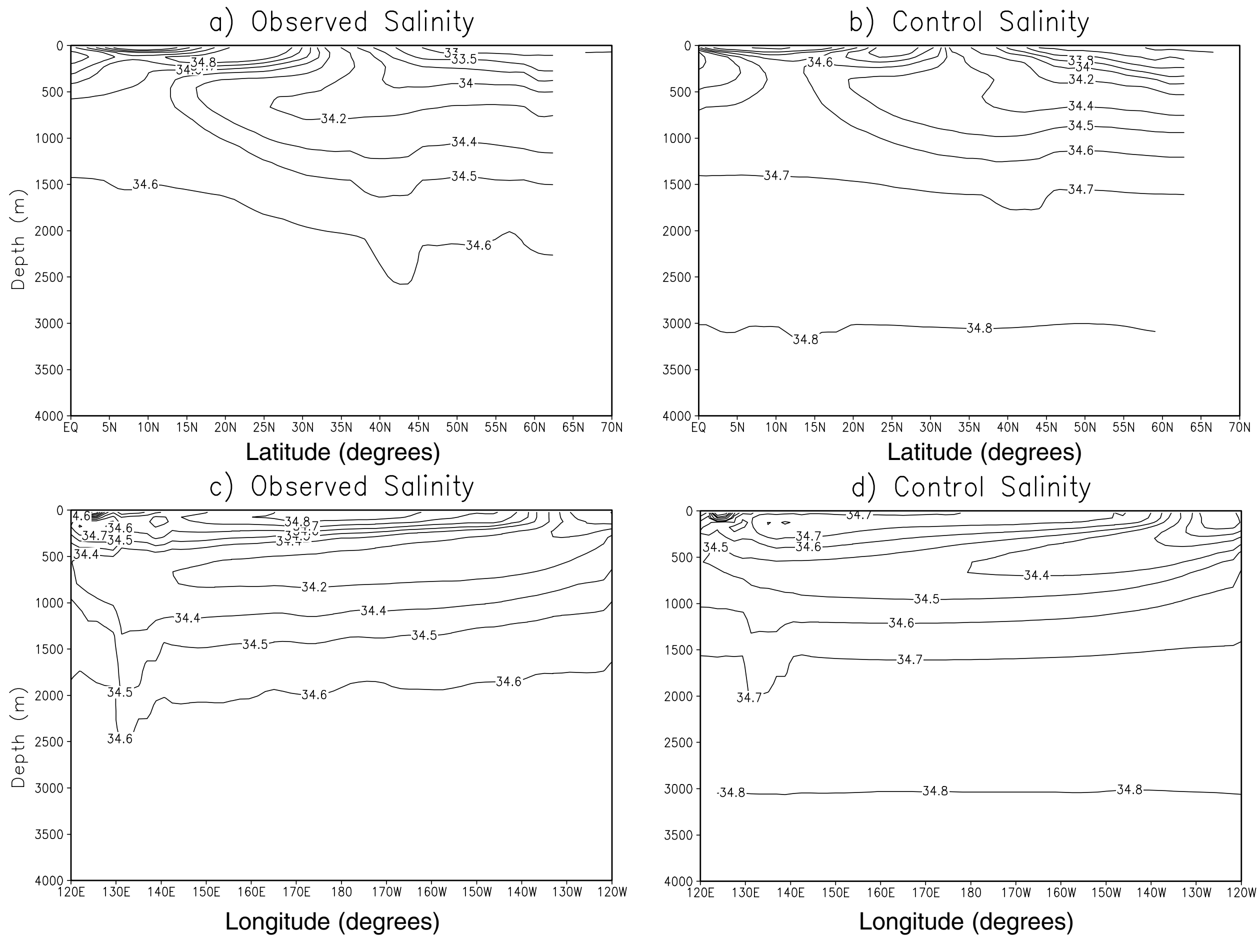

Fig. 1 a) Observations and b) control simulations of annual mean meridional sections of salinity zonally averaged over the Pacific. c) Observations and d) control simulations for annual mean zonal sections of salinity averaged between 20° and 40°N. The observations are taken from Levitus and Boyer (1994).

observed potential temperature at the subarctic front and NPIW ranges from about 6°–10°C, whereas in the simulation the potential temperature of the NPIW is warmer by about 2°C. Again the warmer intermediate water, typical of the simulation, is due to the warmer surface and deep waters.

Figure 3 shows the meridional sections of the simulated glacial salinity and potential temperature and their changes from the control simulation. The glacial salinity and temperature sections are quite different from present-day conditions. First, salinity is greater except for the deep ocean, especially near the surface at high latitudes, where salinity increases by more than 2 psu. As shown later, the salinity increase originates from the Sea of Okhotsk and the western Bering Sea. Even though the salinity increase at high northern latitudes is substantial in the glacial simulation, the salinity at upper and intermediate depths is still lower than that in deep waters as suggested by Keigwin (1998).

Second, potential temperature in the glacial simulation is lower throughout the entire water column, as would be expected. The temperature reduction is substantial in the upper water column, shallower than 300 m from about 20°N to 50°N, especially at about 40°N due to a southward shift of the subtropical gyre, as illustrated later. To the north of 50°N, surface temperature reduction is relatively small because the high latitude ocean temperature is already low. In deep layers below 2000 m, potential temperature decreases to less than 0°C and it becomes less than –1°C below 3000 m. Boyle (2002) compiled glacial temperatures and salinity of ocean deep water and reported that the potential temperature in the Pacific deep water is about –1.3°C and that salinity is lower than in the Antarctic during the glacial period by about 1.0 psu within some range of uncertainty. The simulated glacial deep ocean temperature is close to this proxy estimate. Kim (2004b) showed that the simulated deep ocean salinity in the Pacific is lower than in the Antarctic for the glacial run and this result is qualitatively consistent with the observed proxy estimate.

Third, there is a signature of vertical mixing to the north of the subarctic front showing steep isohalines and isotherms with low salinity. The relatively low salinity water originating from the northern North Pacific propagates to the south and the fresh tongue approaches the equator. The potential temperature of this water mass is less than 2°C. The relatively cold and fresh water mass is compatible with NPIW in the control simulation.

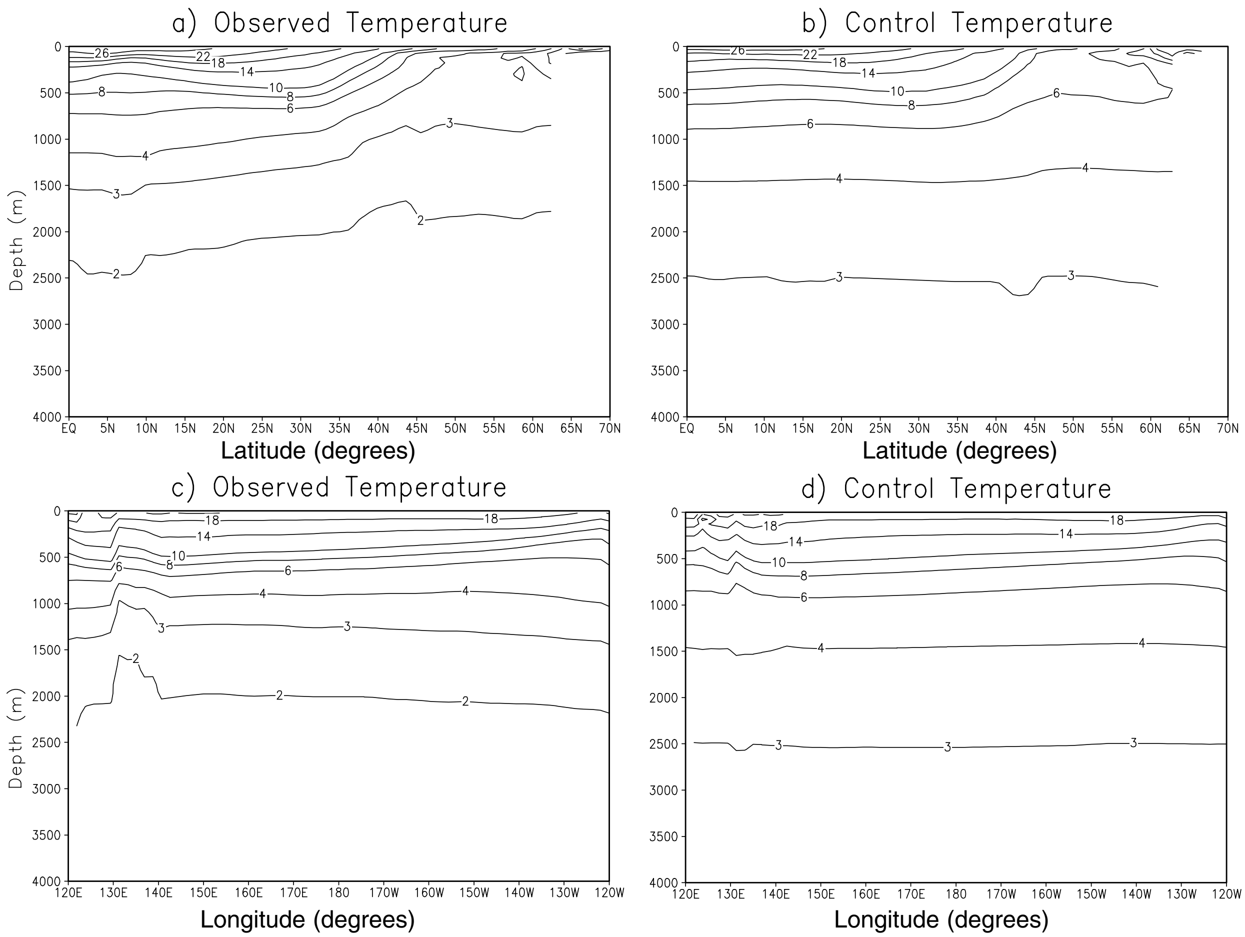

Fig. 2 a) Observations and b) control simulations of annual mean meridional sections of potential temperature zonally averaged over the Pacific. c) Observations and d) control simulations of annual mean zonal sections of potential temperature averaged between 20° and 40°N. The observations are taken from Levitus and Boyer (1994).

Figure 4 displays the zonal sections of salinity and potential temperature averaged between 20° and 40°N from the glacial simulation. The upper layer salinity maximum found in the meridional section at 25°N is located in the western Pacific between 140° and 160°E. The salinity minimum layers associated with NPIW in the control simulation are found at levels shallower than 1000 m; in the glacial simulation they are located at deeper levels, around 2000 m, and on the western side of the Pacific.

The change in salinity and potential temperature leads to a change in potential density. Figure 5 displays the meridional potential density distribution in the control and glacial experiments and the changes in the upper layers. In the control simulation, the North Pacific is strongly stratified as would be expected from the low salinity at high latitudes and relatively high temperature at low to mid-latitudes (Figs 1 and 2). It has long been known that the potential density of the NPIW salinity minimum tongue ranges from 26.7–26.9 kg m^{-3} (Reid, 1965; Talley, 1993; Talley et al., 1995; Yasuda et al., 1996) and does not outcrop (Reid, 1965). This is a different feature from other intermediate waters with a salinity minimum such as AAIW (Talley, 1993). In the control simulation, the NPIW potential density surfaces do not outcrop, which is consistent with observations.

In the glacial simulation, the increase in salinity and decrease in potential temperature leads to a substantial increase in potential density, especially in the upper layers (Figs 5b and 5c). The largest density increase of more than 2 kg m^{-3} is found south of 35°N and north of 60°N. The density increase at high latitudes weakens the vertical stability substantially. Isopycnals become steep so that the 27.6 kg m^{-3} isopycnal comes close to the surface.

In order to confirm which property has more effect on the total change in potential density, we distinguish the density due to the change in temperature and salinity. Because potential density is a function of salinity (S), potential temperature (θ), and pressure (p), we can represent density as $\sigma_\theta = \sigma(S, \theta, p)$. Because p is the same for the two cases and does not influence the change in potential density, the differential can be represented as:

$$\delta\sigma_\theta = S\delta\theta + \theta\delta S + n,$$

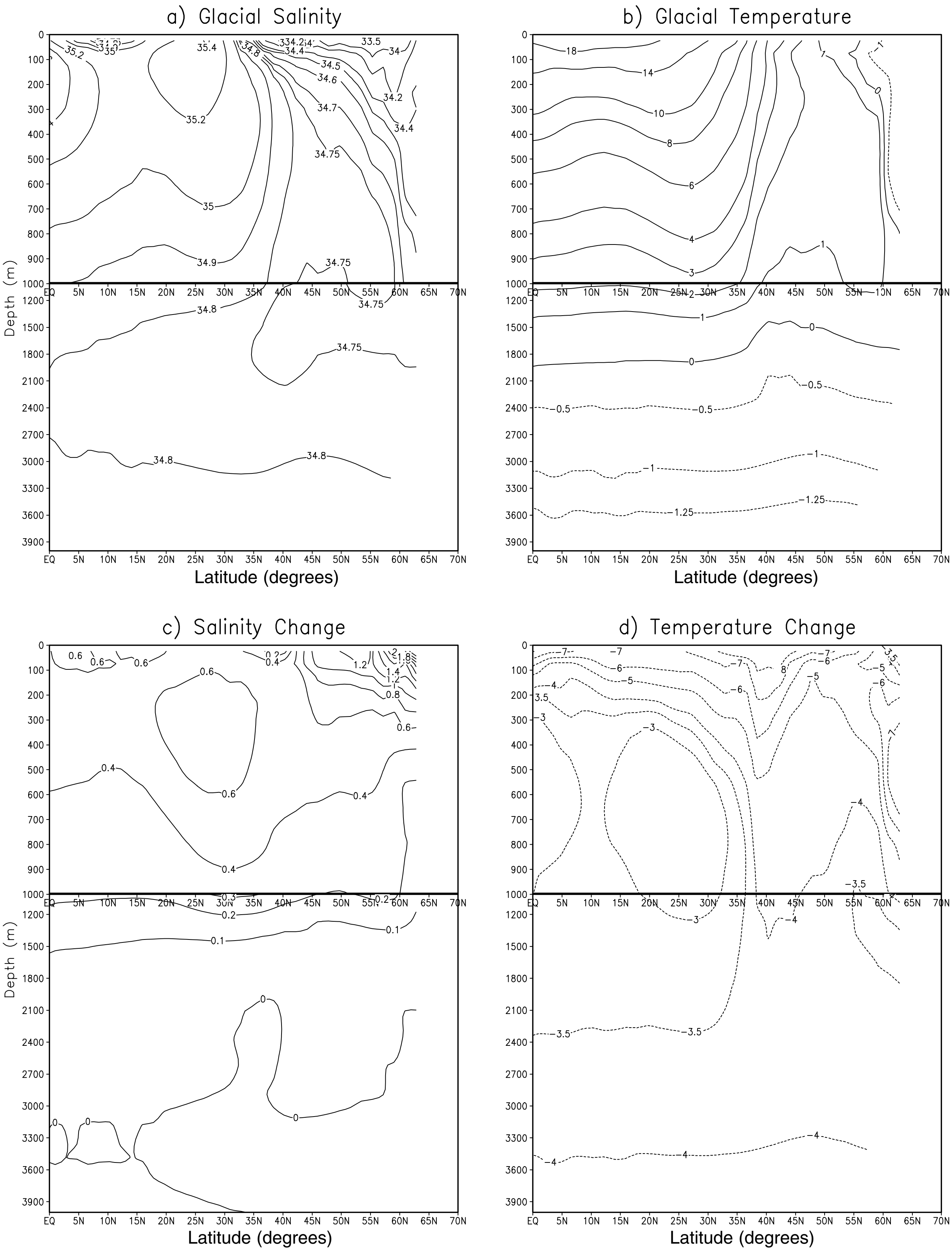

Fig. 3 Zonally averaged annual-mean meridional sections over the Pacific for a) salinity and b) potential temperature simulated in the glacial experiment, and the change between the glacial and control experiments for c) salinity and d) potential temperature.

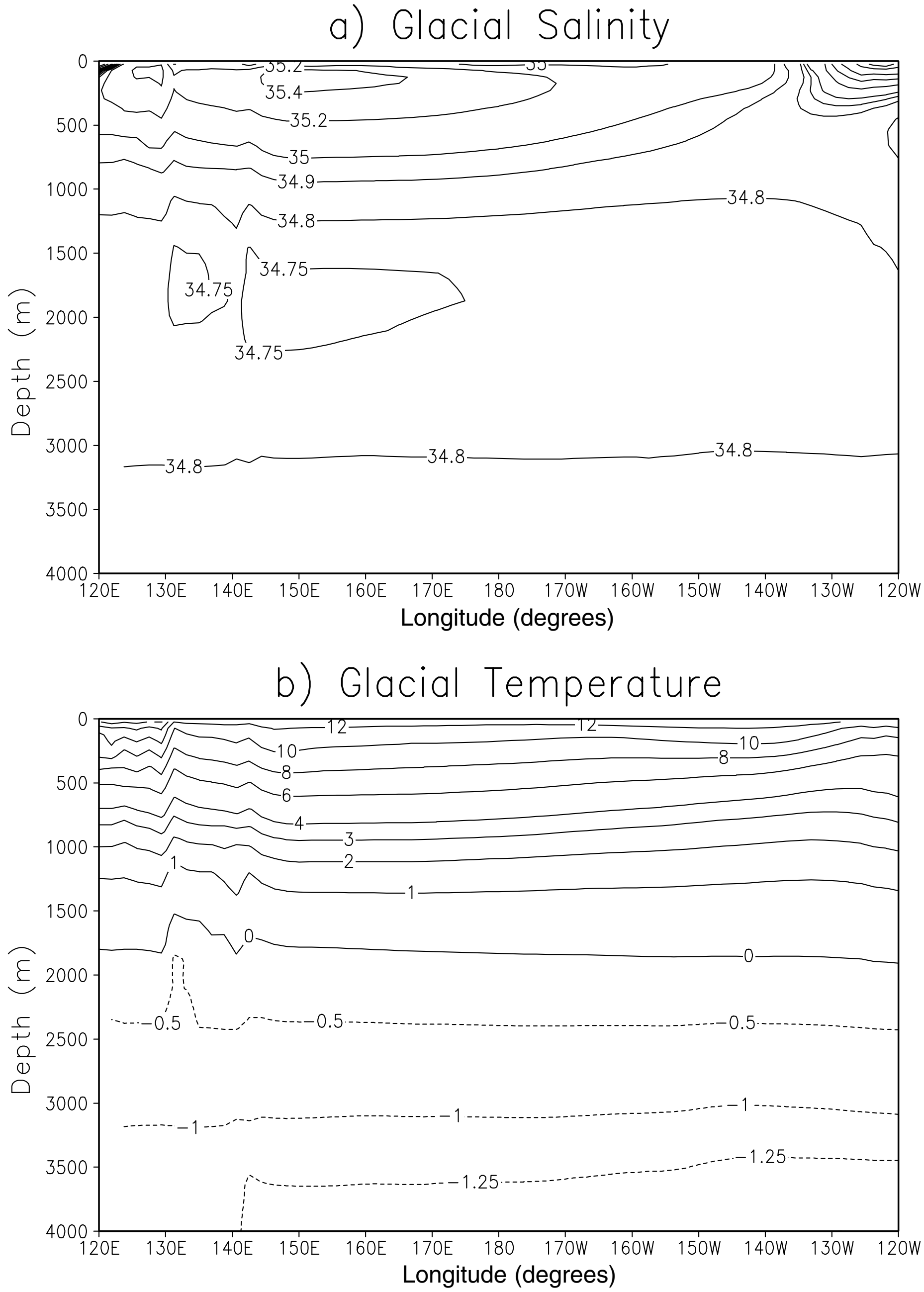

Fig. 4 Annual-mean zonal sections averaged between 20°–40°N for a) salinity and b) potential temperature simulated in the glacial experiment.

where the first term on the right-hand side represents the change in potential density due to potential temperature, the second term represents the change due to salinity, and the third term represents the change due to higher degree non-linear terms. The left-hand side is shown in Fig. 5c and the three terms in the right-hand side are shown in Fig. 6. The decomposition shows that south of about 50°N the temperature reduction plays a dominant role in increasing the glacial potential density, whereas north of about 55°N the increase in salinity plays the dominant role in increasing the density because the increase in salinity is greater to the north. The non-linear effect of temperature and salinity appears to play a minor role, being one or two orders of magnitude lower. This analysis suggests that the increase in salinity is mainly responsible for the weakening of stability in the northern North Pacific in the glacial simulation.

The density increase in the upper layers of the northern North Pacific and associated weaker stability imply that there must be some change in thermohaline circulation. Figure 7 shows the North Pacific overturning circulation obtained in the control and glacial simulations. In the control run, the strong positive cell at low latitudes is associated with the wind-driven subtropical circulation, while the negative cell at mid-latitudes is associated with the subpolar gyre. The

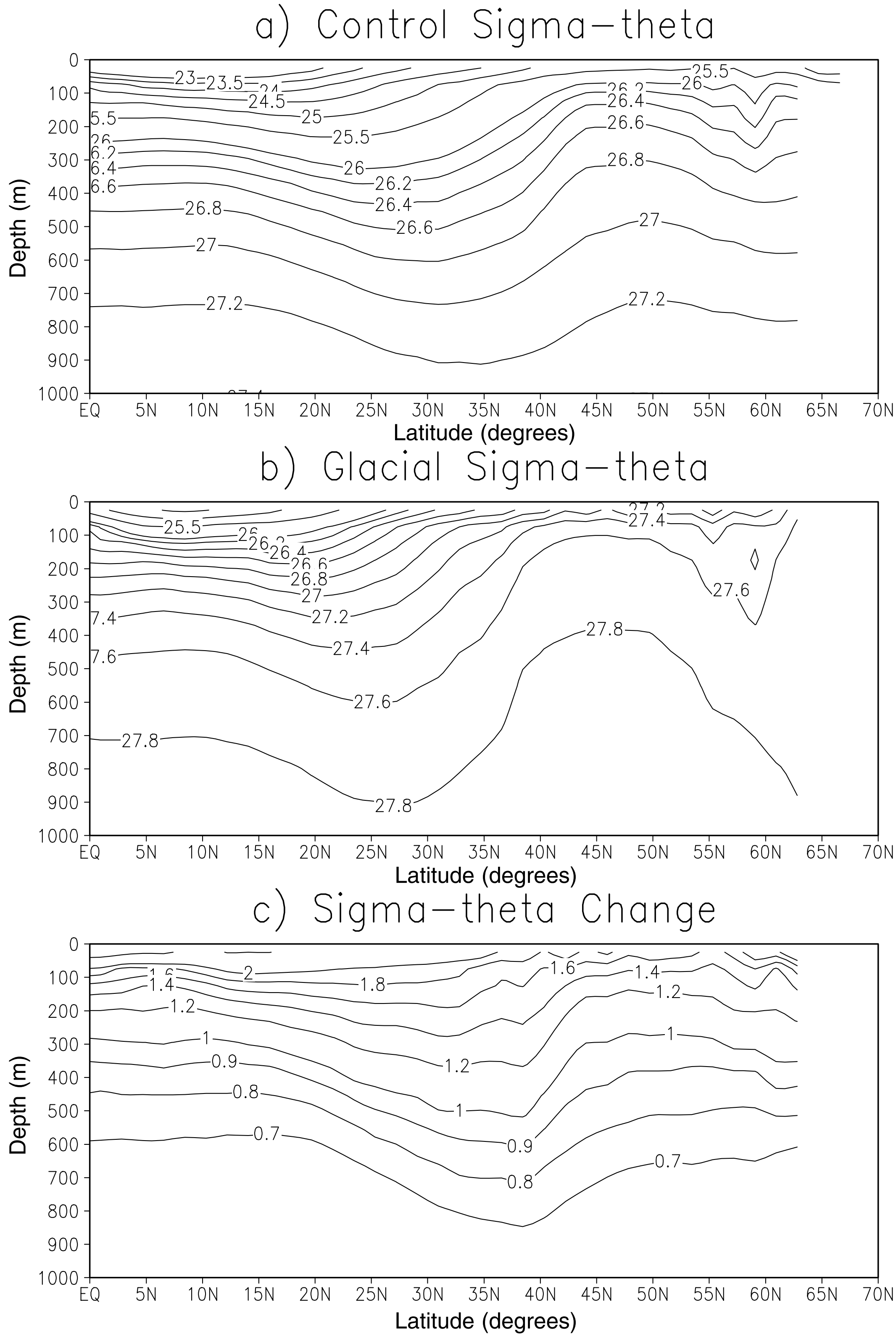

Fig. 5 Annual-mean meridional sections zonally averaged over the Pacific of the potential density (σ_θ) for a) the control experiment, b) the glacial experiment, and c) the changes between the control and glacial experiments. (Units are kg m^{-3}.)

positive cell at high northern latitudes and depths between 300–500 m is related to the NPIW production, which is about 2 Sv in the control simulation, consistent with observations (Macdonald, 1998; Talley, 2003). The negative cell reaching the bottom at low latitudes is the northward outflow of AABW.

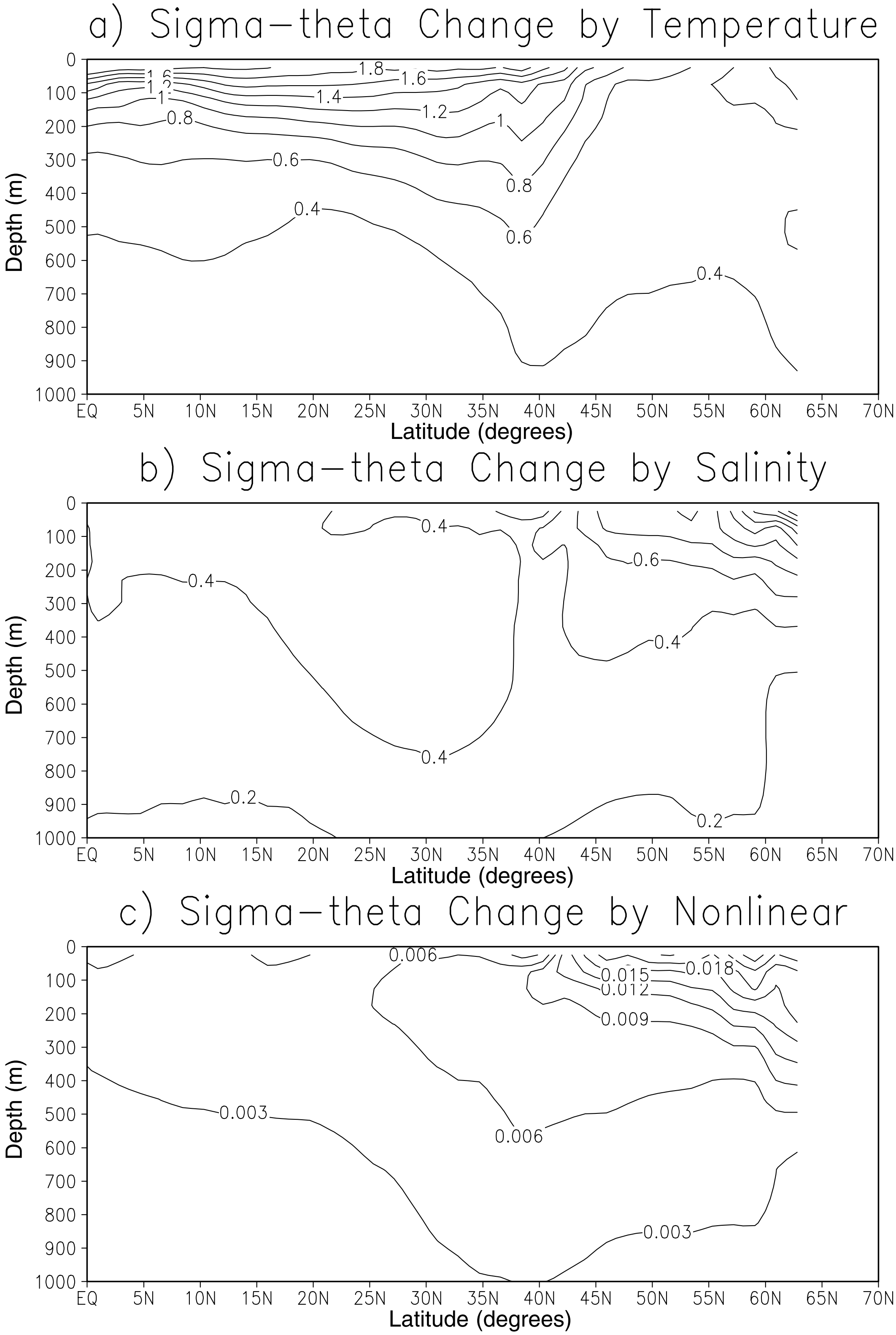

Fig. 6 Annual-mean meridional sections zonally averaged over the Pacific of the change in potential density (σ_θ) change due to a) temperature, b) salinity, and c) the non-linear term. (Units are in kg m^{-3}.)

In the glacial simulation, circulations associated with both the subtropical and subpolar gyres are intensified due to an increase in surface wind in the North Pacific sector (Kim et al., 2003). The NPIW production increases to 3 Sv and its outflow reaches deeper layers, up to more than 2000 m, consistent with the water mass propagation tongue seen in Figs 3a

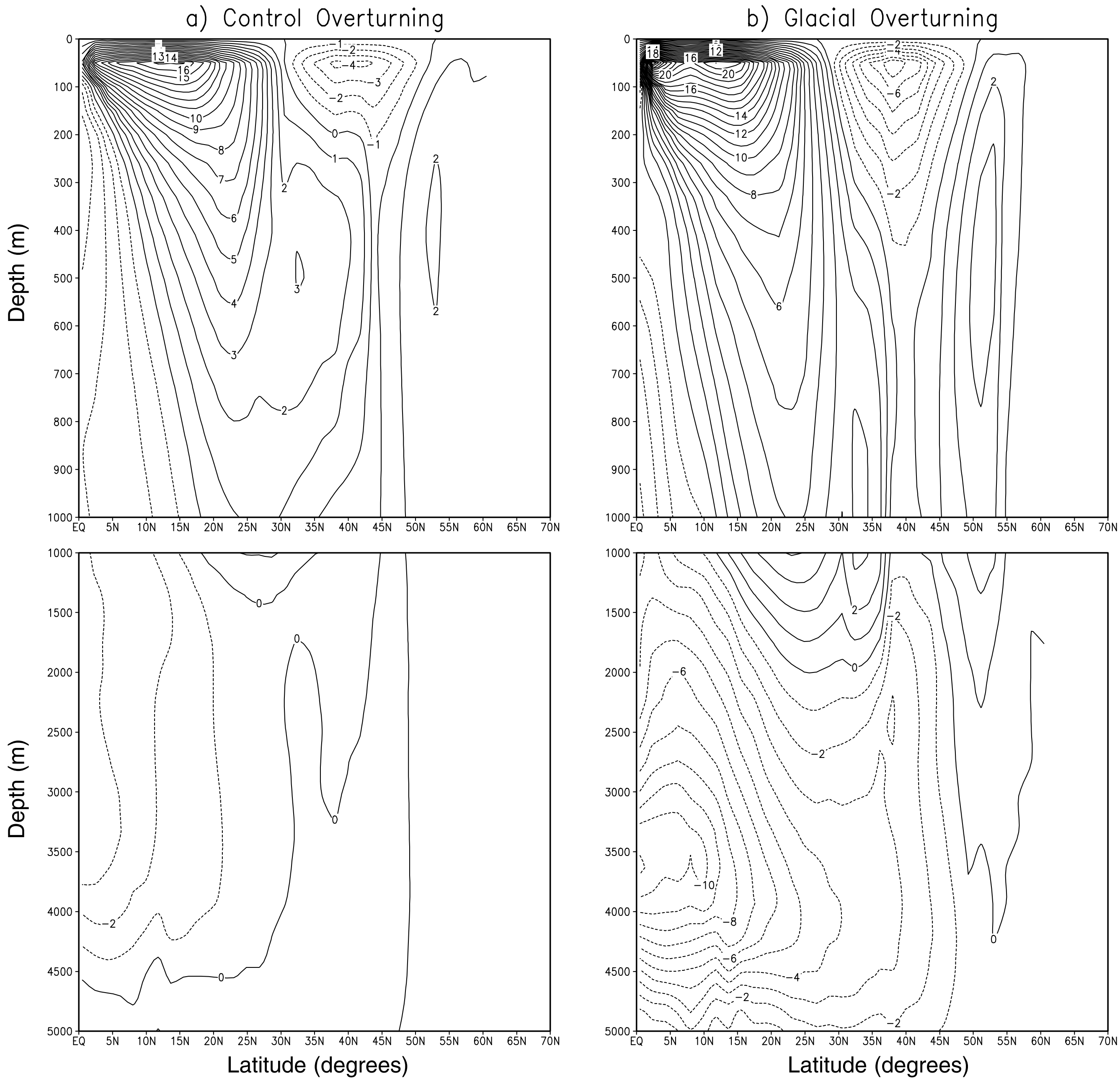

Fig. 7 Annual-mean meridional streamfunction for the North Pacific domain simulated in a) the control experiment and b) the glacial experiment. (Units are Sv (10^6 m^3 s^{-1}).)

and 4a. The AABW outflow is much more intensified and extends farther to the north in the glacial simulation than in the control case. The stronger and deeper NPIW (or glacial North Pacific Deep Water) production and the more extensive AABW outflow obtained in the glacial simulation are consistent with that suggested by proxy evidence (see Section 1).

In order to examine how far NPIW propagates to the south in the control and glacial simulations, we examine the meridional velocities averaged over 20°–40°N and 0°–20°N (Fig. 8). In the control case, the southward propagation is widespread and covers almost the entire Pacific basin reaching depths up to 1500 m in the northern latitudes, but it becomes shallower towards the south, presumably due to the northward propagation of the water mass originating in the Southern Ocean below the NPIW. At low latitudes, there is a western boundary current tongue at about 1500 m. In the glacial case, the southward circulation is deeper than in the control simulation, reaching more than 3000 m in northern latitudes. As in the control case, the southward flow shoals towards southern latitudes. In the glacial simulation, the western boundary current becomes much stronger and deeper, reaching depths greater than 3000 m.

The weakening of the vertical stratification in the glacial simulation over the northern North Pacific, evident in Fig. 5,

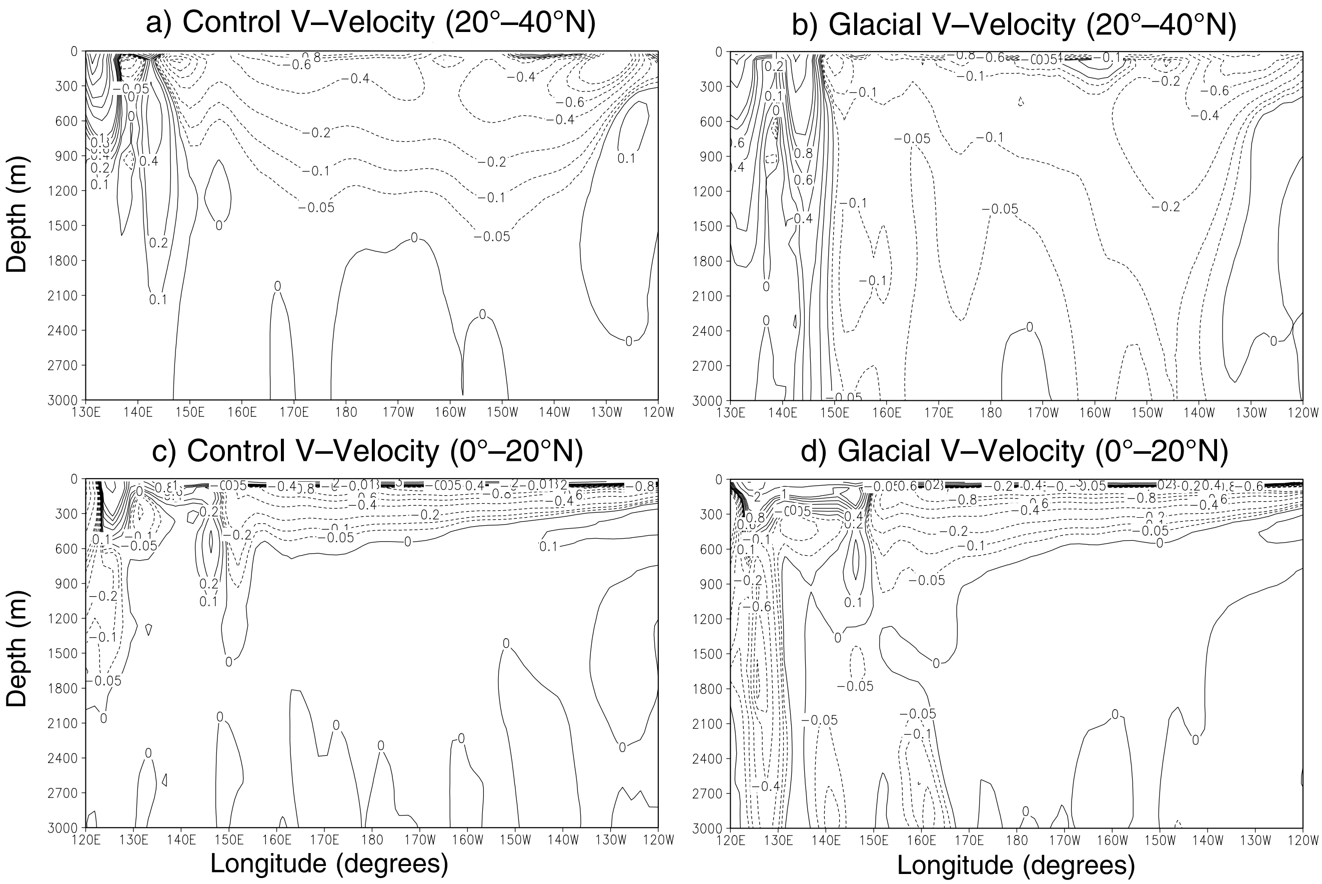

Fig. 8 Annual-mean zonal sections of the meridional velocities, averaged between 20° and 40°N, simulated in a) the control experiment, b) the glacial experiment and, averaged between 0° and 20°N, simulated in c) the control experiment and d) the glacial experiment.

intensifies the formation of NPIW and subsequently strengthens and deepens the North Pacific overturning circulation. This weaker vertical stratification is due to a relatively greater increase in surface salinity at high northern latitudes in the Pacific than at greater depths, as shown in Fig. 3c, and than the southern part of the of the North Pacific, as shown in Fig. 9, which presents the change in surface salinity and temperature between the two experiments. In the glacial simulation, a large increase in surface salinity is seen in most of the North Pacific. The salinity increase is especially large in the northern and eastern Sea of Okhotsk and the western Bering Sea. In those areas, salinity increases by more than 2.4 psu to become as large as about 34.4 psu. Warren (1983) suggested that for deep convection to reach 1000 m and 2000 m, surface salinity should be at least 34.08 psu and 34.39 psu, respectively. The simulated glacial salinities are within this range. The Sea of Okhotsk and the western Bering Sea are suggested as possible glacial deep water source regions as in Boyle (1997). In the western Sea of Okhotsk, the salinity increase is smaller than in the eastern region. This seems to be associated with the increase in river discharge from the Amur River in the glacial simulation, illustrated later. In low to mid-latitudes, surface salinity increases overall associated with a change in the hydrological budget. There is a narrow region of salinity reduction at about 40°N. This is due to precipitation exceeding evaporation and the southward shift of the subtropical gyre as shown later.

With glacial conditions, surface temperature decreases everywhere in the North Pacific as would be expected (Fig. 9b). Several studies based on geological records suggest that the northern edge of the subtropical gyre moved southward during the glacial period (Kent et al., 1971; Sawada and Handa, 1998; Tanimura, 1999; Lee and Park, 2003). The simulated control barotropic streamfunction displayed in Fig. 10 shows that the northern edge of the subtropical gyre is at about 43°N but in the glacial simulation the boundary moved southward and is found at about 40°N consistent with the observational proxy evidence. This southward shift of the gyre would result in a marked temperature drop along the Kuroshio Current to the south of Japan and the northern boundary of the gyre along 40°N. The southward movement of the subtropical gyre is, in part, due to the change in zonal-mean wind stress, which is displaced to the south by about 3° in the glacial simulation (Fig. 11a), associated with the southward shift of the Aleutian low pressure centre (Fig. 11b).

Another area of marked cooling is the East/Japan Sea where the surface is cooled by more than 10°C. In the control simulation, sea surface temperature (SST) in the southern part of the East/Japan Sea ranges from 10° to 16°C (not shown), which is comparable with observations (Chu et al., 2001;

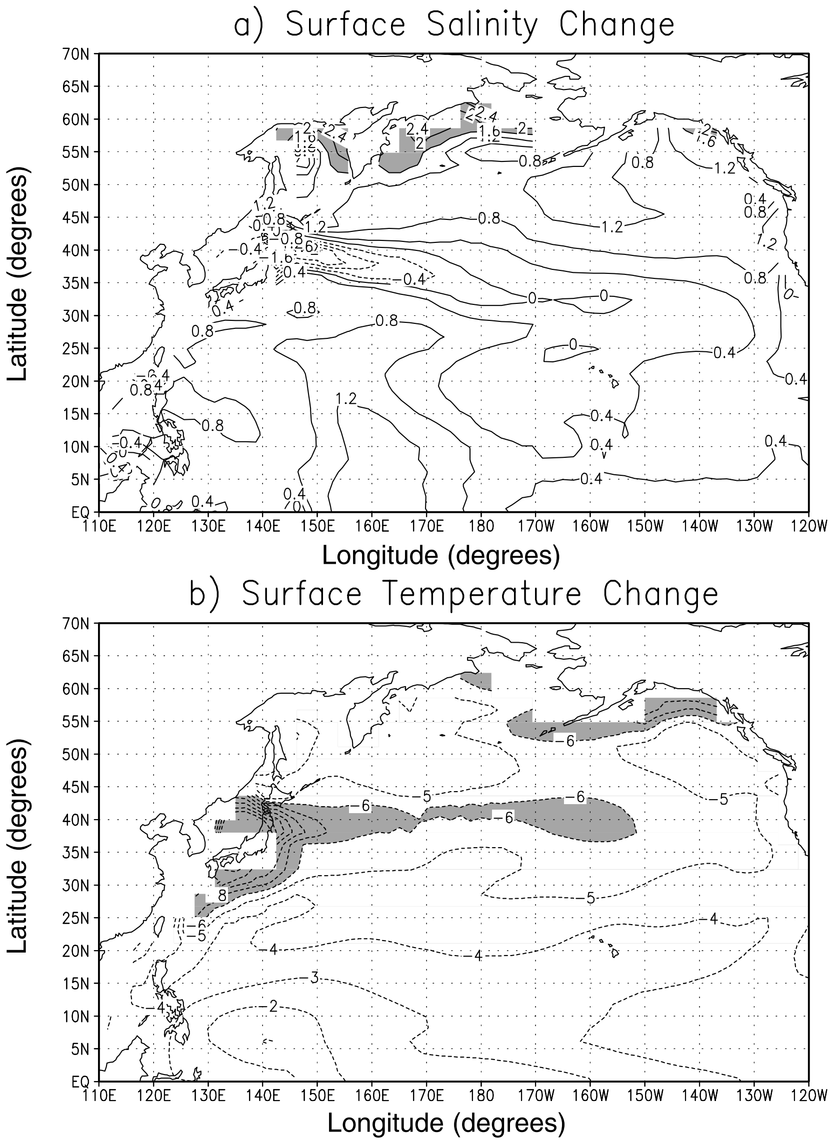

Fig. 9 Geographic distribution of the change in annual-mean surface a) salinity and b) temperature in the North Pacific. Glacial salinity increases of more than 1.6 psu and temperature reductions of more than 6°C are shaded.

Morimoto and Yanagi, 2001). The relatively high temperature here is due to the inflow of the Tsushima warm current through the Korea Strait as a branch of the Kuroshio Current. In the glacial simulation, on the other hand, the Tsushima warm current was largely restricted and only partly allowed due to the sea level drop (approximately 130 m). The limitation of the warm water influx to the East/Japan Sea leads to substantial cooling in the glacial simulation. The marked surface cooling in these regions is also found in the CLIMAP (1981) reconstruction, which shows a cooling of up to 8°C in August.

The spatial pattern of the surface ocean in the North Pacific in the glacial simulation is consistent overall with the CLIMAP (1981) reconstruction, but the degree of cooling is larger in the simulation, although the CLIMAP reconstructions of surface ocean temperature are believed to be overestimated as shown by a recent evaluation of the Paleoclimate Modelling Intercomparison Project (PMIP) and other model simulations (Kageyama et al. (2006) and references therein). A more detailed description of the glacial SST change is found in Kim et al. (2002, 2003).

Because the increase in surface salinity in the Sea of Okhotsk and the western Bering Sea is crucial in driving the glacial NPIW production, we examine possible reasons for the increase in surface salinity in those regions. First, the marked surface cooling enhances sea-ice growth. Figure 12 shows the annual mean distribution of sea-ice thickness in the control and glacial simulations. In the control simulation, thin sea ice is found in the Sea of Okhotsk and the western Bering Sea. Some authors suggest that, at present, brine rejection occurs in the northwestern and northern shelves of the Sea of Okhotsk and this is a probable place for the formation of NPIW (Kitani, 1973; Talley, 1991, 1993; Martin et al., 1998; Gladyshev et al., 2000). Recently Shcherbina et al.

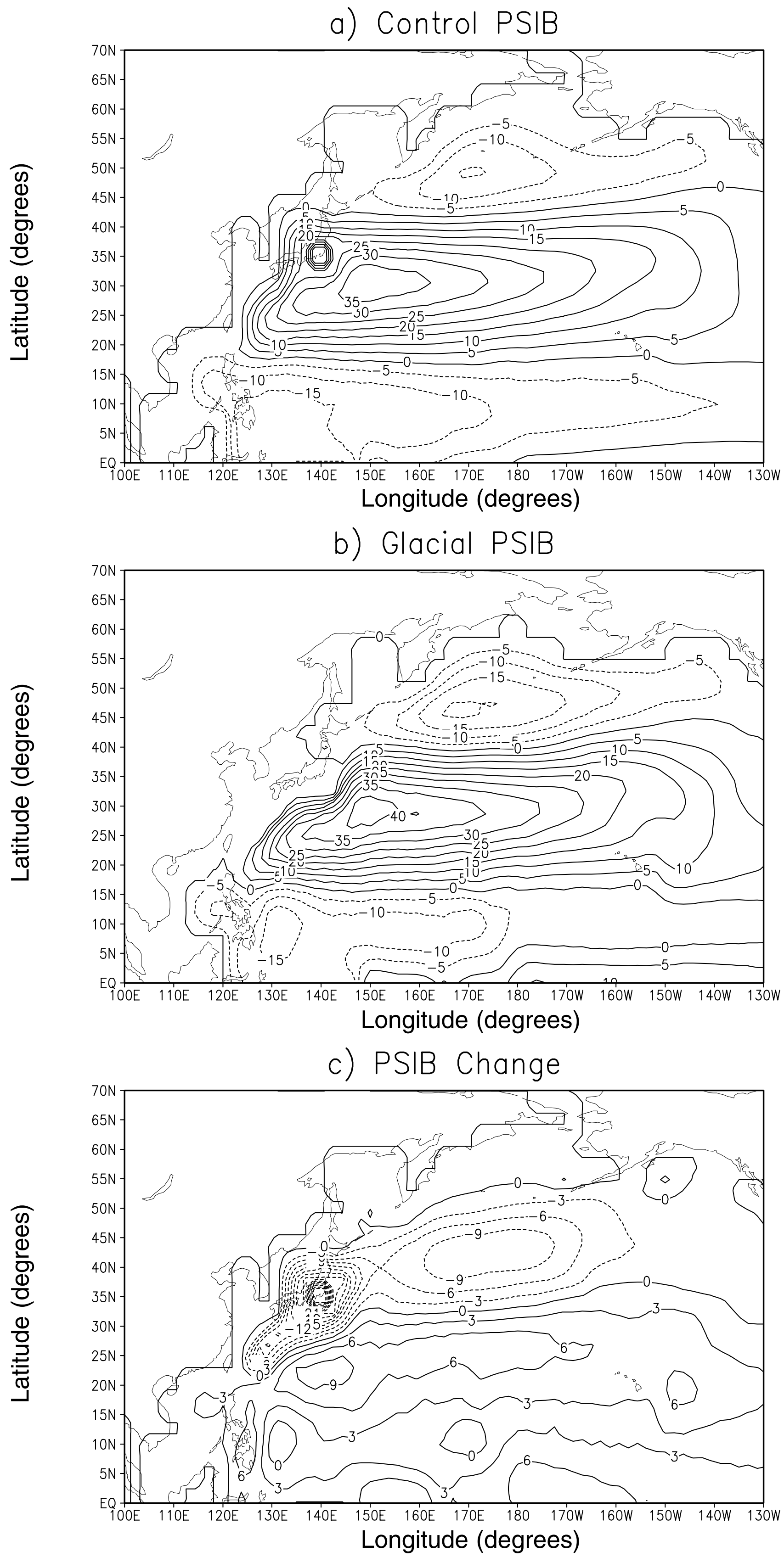

Fig. 10 Annual mean barotropic streamfunction for the North Pacific domain simulated in a) the control experiment, b) the glacial experiment, and c) the change. (Units are Sv (10^6 m^3 s^{-1}).)

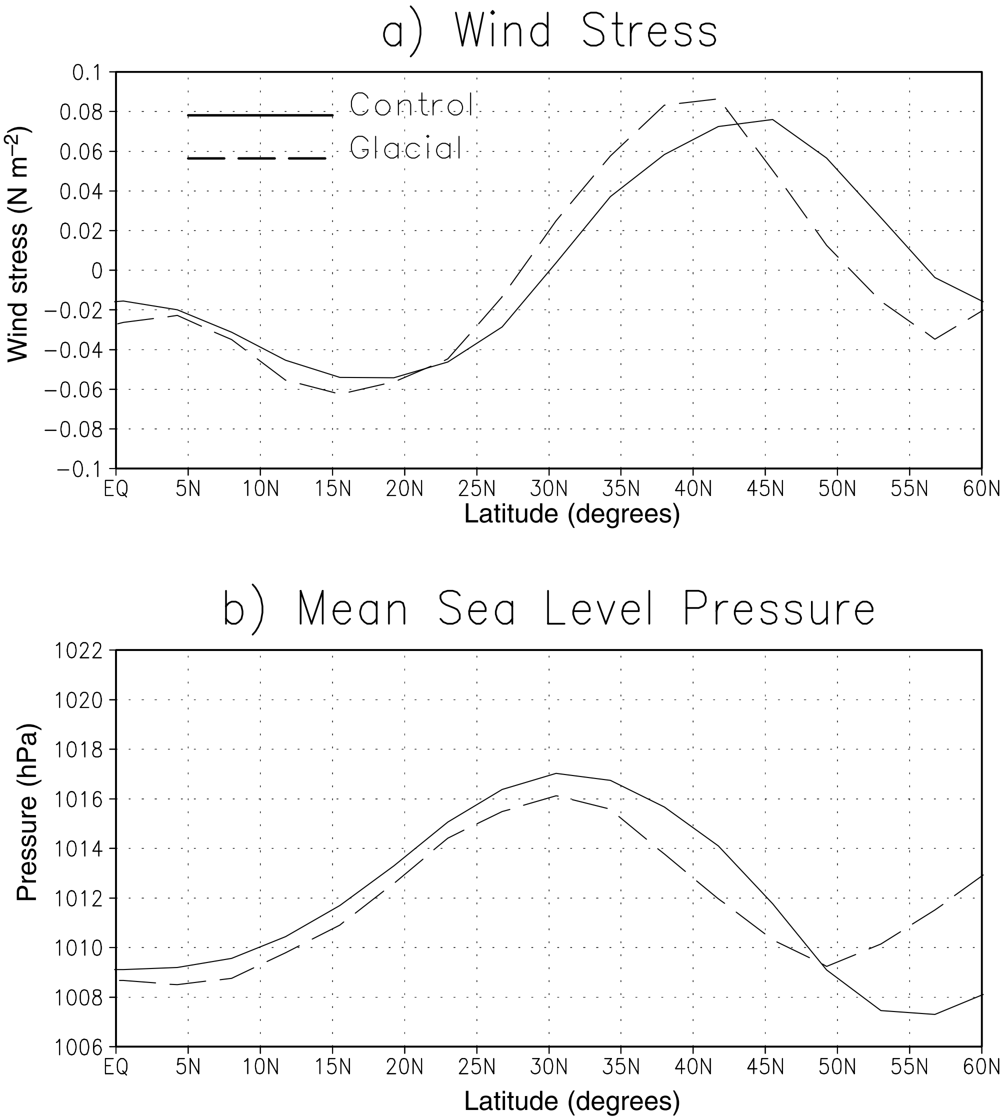

Fig. 11 Annual and zonal mean over the Pacific for a) the wind stress, and b) mean sea level pressure.

(2003) found a substantial increase in bottom salinity by brine rejection during an ice-covered period in the northwestern Sea of Okhotsk. In the glacial simulation, sea ice becomes thicker and more extensive covering a large portion of the northwestern Pacific Ocean. Sea ice is especially thick in the northwestern Sea of Okhotsk and the western Bering Sea, where brine release from sea-ice formation might contribute to the marked increase in sea surface salinity shown in Fig. 9a. In the glacial simulation, the southern margin of sea ice reaches northern Japan. By analyzing ice-rafted debris in fine sediment cores, Ikehara (2003) found that during the glacial period the southern margin of seasonal sea ice was probably located in the vicinity of the Matsumae Plateau and occasionally extended further south to near the Oga Peninsula at about 40°N. The simulation slightly overestimates the southern extent of sea ice.

Second, in addition to brine release, a change in the hydrological budget plays an important role in increasing surface salinity. In the present ocean, the low salinity of surface water in the northern North Pacific is mainly due to a small regional evaporation rate, which allows a net freshwater input to the surface layer from precipitation and runoff (Warren, 1983). The low evaporation rate is due, in turn, to the relatively low surface temperature. Figure 13 displays the changes in precipitation minus evaporation (P-E), precipitation, and evaporation. In the glacial simulation, both precipitation and evaporation decrease in the northern North Pacific. The reduction in precipitation is due both to the reduction in evaporation associated with surface cooling and to the reduction in horizontal advection of water vapour. The precipitation decrease in the northern North Pacific in the glacial simulation is consistent with other coupled model simulations reported based on recent PMIP2 results (Yanase and Abe-Ouchi, 2007). In most of the North Pacific, the reduction in precipitation is larger than the reduction in evaporation by about 0.5 mm per day on average. If the excessive freshwater

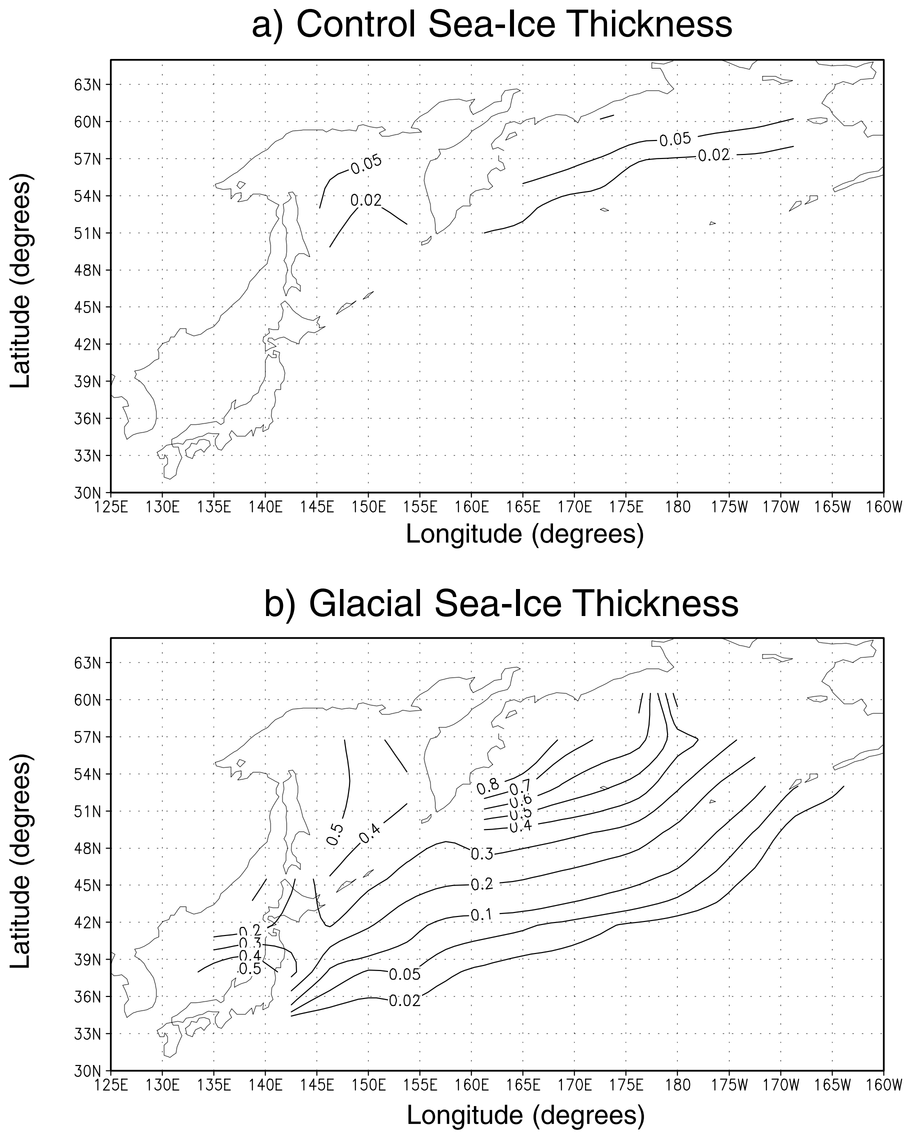

Fig. 12 Geographic distribution of the annual-mean sea-ice thickness simulated in a) the control experiment and b) the glacial experiment. (Units are metres.)

deficit is accumulated within a surface wind mixed layer of about 100 m for 10 years (a time scale during which the water column travels round the subpolar gyre once), then the height of the water column would decrease by about 1.8 m. The salinity would then rise by about 1.8%, which is about 0.6 psu. This is a simple estimate by assuming a 10-year mixing time in the upper mixed layer, and the results would vary depending on mixing time and depth.

Third, a change in river runoff modifies surface salinity. Several rivers influence the freshwater budget in the northern North Pacific. The Yukon and Amur rivers directly influence the Bering Sea and the Sea of Okhotsk, respectively, and the Columbia and Yangtze rivers have an indirect influence. Kim et al. (2003) reported that there was a reduction in river discharge in the Yukon River by 78% (11,000 $m^3 s^{-1}$), but in the Amur River it increases by 80% (5500 $m^3 s^{-1}$) in the glacial simulation. In the Yangtze and Columbia rivers, the river discharge decreases by 24% and 13%, respectively. In total, river discharge to the North Pacific was reduced by 8900 $m^3 s^{-1}$ in the glacial simulation and the reduction in the Yukon River discharge to the Bering Sea, which is due to a drier glacial climate over Alaska and also partly due to the presence of the Cordillerian ice sheet, plays the most significant role in increasing surface salinity. If the net reduction in river discharge (5500 $m^3 s^{-1}$) from the Yukon and Amur rivers modifies the salinity of the surface mixed layer (100 m) within the subpolar gyre, whose area is about 70 degrees in longitude and about 15 degrees in latitude, for 10 years (the advective time scale of the gyres) then it accounts for about a 0.2% increase in salinity, which is about 0.1 psu. This estimate suggests that the change in the local P-E budget plays a more important role in increasing salinity in the northern North Pacific than the change in river discharge.

Finally, a change in vertical mixing and horizontal advection affects surface salinity. As displayed in Fig. 10, the subpolar gyre is stronger in the glacial simulation and more salt

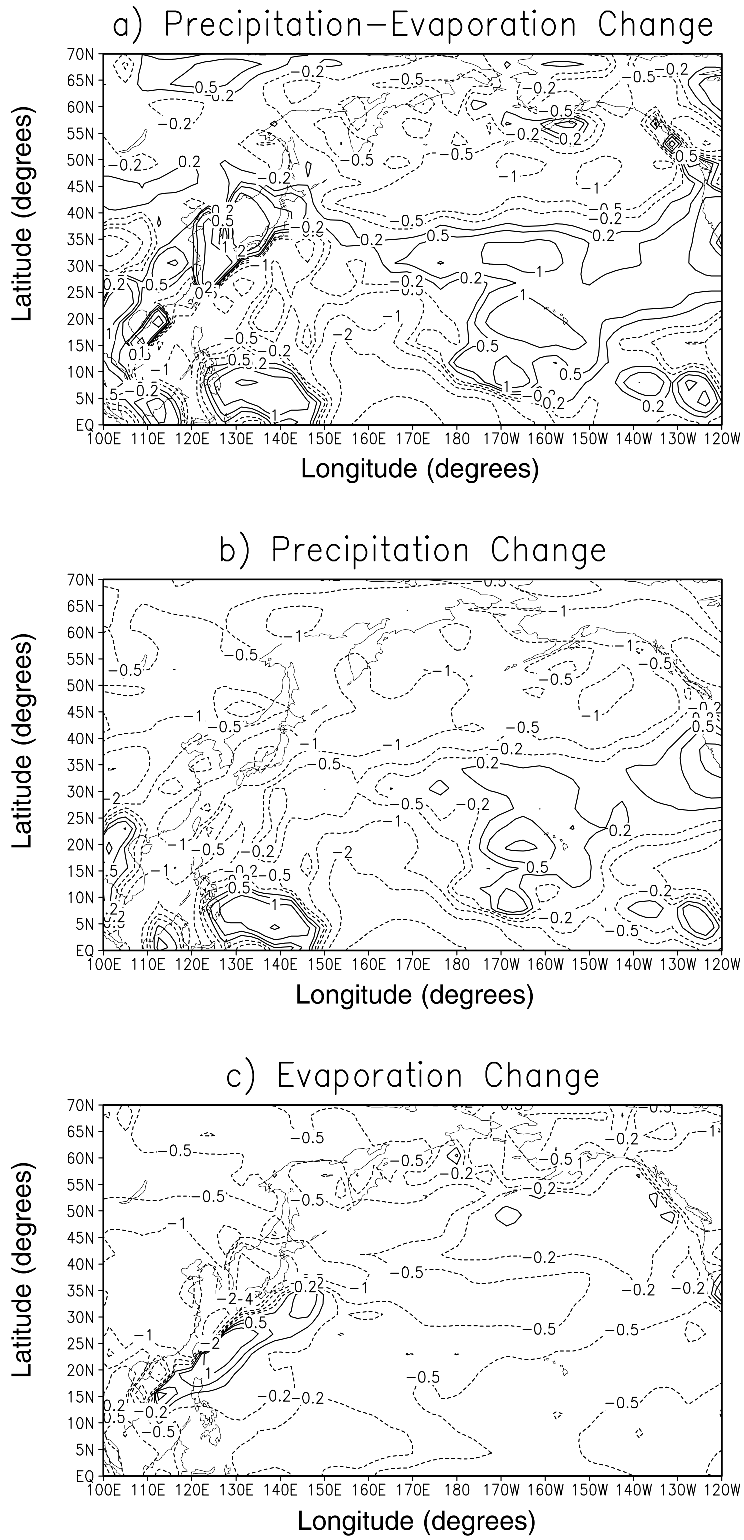

Fig. 13 Geographic distribution of the change in annual mean a) precipitation minus evaporation, b) precipitation, and c) evaporation. (Units are mm day^{-1}.)

would be transported from the subtropics where salinity is higher. The deeper and stronger glacial North Pacific overturning would enhance vertical mixing between the fresher surface water and saltier deep water to raise the surface salinity while lowering the salinity in the deep water. Figure 3c clearly shows a decrease in salinity in the lower part of the overturning cell that lies between 3000 and 4000 m.

The stronger NPIW production due to the increase in surface salinity may influence or may be influenced by the deep water production in other ocean basins. Several studies have shown that there is an interbasin see-saw effect, over long time scales, of deep water formation in the North Pacific, Southern, and Atlantic oceans suggesting that there is an interdependence (Broecker, 2000; Seidov et al., 2001; Seidov and Haupt, 2003; Saenko et al., 2004). Using a sensitivity experiment, Saenko et al. (2004) showed that the reduction in the freshwater supply to the North Pacific results in decreased salinity and an associated meridional overturning circulation in the Atlantic, and vice versa, due to a positive feedback between ocean circulation and salinity. In this study, the increase in surface salinity and associated overturning circulation in the North Pacific accompanies the substantial reduction in surface salinity and overturning circulation in the Atlantic Ocean as described in Kim et al. (2003). Although it is hard to determine which basin influences which, the change in glacial overturning circulation in the present study is consistent with that of Saenko et al. (2004). In the glacial experiment, AAIW production is almost absent, whereas AABW production and its outflow is substantially enhanced due to the increase in surface salinity around the Southern Ocean (Kim, 2004b). The enhanced AABW formation and its outflow fills the Atlantic basin almost entirely in response to the weakening of the Atlantic overturning circulation, whereas in the Pacific both the AABW outflow and NPIW outflow appear to be stronger.

4 Summary and conclusions

The glacial change in ocean properties and circulation in the North Pacific has been investigated using the CCCma atmosphere-ocean-sea-ice coupled model. The control climate simulation reproduces observed features such as the NPIW low salinity tongue, subarctic front, high salinity subtropical water, etc. reasonably well, even though salinity and potential temperature are slightly overestimated in comparison to observations. The simulated NPIW production for present-day conditions is about 2 Sv, located between 300–600 m, which is consistent with observations.

Upon implementing the glacial boundary conditions, salinity in the upper layers of the North Pacific markedly increases, whereas deep water salinity decreases slightly due to vertical mixing. Potential temperature decreases throughout the entire water column with a substantial decrease in the upper layers at mid-latitudes and in intermediate layers at high latitudes. The deep water temperature approaches the freezing point. The glacial deep water property change is consistent with proxy estimates. In the northern North Pacific, there is a strong vertical mixing signature with a relatively fresh and cold plume up to about 1000 m. The increase in salinity and decrease in temperature leads to the increase in potential density. The increase in potential density is larger in the upper layers than in the deep layers, reducing the stability of the upper water column. Analysis shows that at low latitudes the increase in potential density is due to the reduction in potential temperature, whereas at high latitudes the increase in salinity plays the dominant role in increasing potential density in upper layers.

The weaker glacial water column stability leads to the increase in overturning circulation in the North Pacific. In the glacial simulation, the NPIW production increases to 3 Sv and reaches depths greater than 2000 m and its outflow nears the equator. The AABW outflow is also stronger. This result is consistent with the proxy estimates using carbon isotopes and cadmium concentration, which were lower in the northwestern Pacific, but were almost unchanged in the western equatorial Pacific.

The change in both salinity and temperature contributes to the increase in density in the upper water column with the increase in salinity having a more dominant role in the northern North Pacific. Surface salinity increase is especially large in the northern and eastern Sea of Okhotsk and the western Bering Sea. Several factors affect surface salinity. First, in the glacial simulation sea ice substantially increases in the northwestern Pacific, which may increase brine release. Second, in the northern North Pacific annual mean evaporation exceeds precipitation, resulting in a drier climate. This is due to a larger reduction in precipitation. Third, river discharge to the Bering Sea from the Yukon River and to the North Pacific from the Yangtze and Columbia rivers is substantially reduced in the glacial simulation. Although river runoff from the Amur River to the Sea of Okhotsk increases, the net change is a substantial reduction. Fourth, the intensified subpolar gyre and vertical mixing increases the surface salinity in the northern North Pacific. All these conditions act together to increase the surface salinity in the northern North Pacific.

In conclusion, the coupled model simulates an enhanced circulation in the intermediate and upper deep layers of the northern North Pacific with glacial boundary conditions, consistent with proxy estimates. The enhanced North Pacific circulation is mainly due to the increase in surface salinity in the Sea of Okhotsk and the Bering Sea through a reduction in freshwater input.

Acknowledgements

This study greatly benefitted from input by colleagues at the Canadian Centre for Climate modelling and analysis (CCCma), we especially acknowledge Greg Flato and George Boer for consistent support and Fouad Majaess, Warren Lee, and Daniel Robitaille for model production. We would also like to thank two anonymous reviewers for their constructive comments. The analysis of the model results was supported by the integrated research on the composition of polar atmosphere and climate change (COMPAC) (PE08030) of the Korea Polar Research Institute, and Polar Science Program (R01-2006-000-10441-0) of the Korea Science and Engineering Foundation. Y.-G. Park was supported by the Korea Ocean Research and Development Institute (KORDI) (PP07401).

References

BOER, G. J.; G. FLATO, M. C. READER and D. RAMSDEN. 2000a. A transient climate change simulation with greenhouse gas and aerosol forcing: experimental design and comparison with the instrumental record for the twentieth century. *Clim. Dyn.* **16**: 405–425.

BOER, G. J.; G. FLATO and D. RAMSDEN. 2000b. A transient climate change simulation with greenhouse gas and aerosol forcing: projected climate to the twenty-first century. *Clim. Dyn.* **16**: 427–450.

BOYLE, E. A. 1992. Cadmium and $\delta^{13}C$ paleochemical ocean distributions during the stage 2 glacial maximum. *Ann. Rev. Earth Planet. Sci.* **20**: 245–287.

BOYLE, E. A. 1997. Characteristics of the deep ocean carbon system during the past 150,000 years: ΣCO_2 distribution, deep water flow patterns, and abrupt climate change. *Proc. Natl. Acad. Sci. USA*, **94**: 8300–8307.

BOYLE, E. A. 2002. Oceanic salt switch. *Science*, **298**: 1724–1725.

BROCCOLI, A. J. 2000. Tropical cooling at the Last Glacial Maximum: An atmosphere-mixed layer ocean model simulation. *J. Clim.* **13**: 951–976.

BROECKER, W. S. 1982. Glacial to interglacial changes in ocean chemistry. *Prog. Oceanogr.* **11**: 151–197.

BROECKER, W. S. 1997. Thermohaline circulation, the Achilles heel of our climate system: Will man-made CO_2 upset the current balance? *Science*, **278**: 1582–1589.

BROECKER, W. S. 2000. Was a change in thermohaline circulation responsible for the Little Ice Age? *Proc. Nat. Acad. Sci.* **97**(4): 1339–1342.

BUSH, A. B. and S. G. PHILANDER. 1999. The climate of the Last Glacial Maximum: Results from a coupled atmosphere-ocean general circulation model. *J. Geophys. Res.* **24**: 24509–24525.

CHU, P. C.; J. LAN and C. FAN. 2001. Japan Sea thermohaline structure and circulation. Part II: A variational P-vector method. *J. Phys. Oceanogr.* **31**: 2886–2902.

CLARK, P. U.; A. C. MIX and E. BARD. 2001. Ice sheets and sea level of the Last Glacial Maximum. *EOS, Transactions AGU*, **82**(22): 241–247.

CLIMAP. 1981. Seasonal reconstructions of the Earth's surface at the last glacial maximum. Geol. Soc. Am. Map Chart Ser. MC-36.

CROWLEY, T. J. and S. K. BAUM. 1997. Effect of vegetation on an ice-age climate model simulation. *J. Geophys. Res.* **102**: 16463–16480.

CURRY, W. B.; J.-C. DUPLESSY, L. D. LABEYRIE and N. J. SHACKLETON. 1988. Changes in distribution of ^{13}C of deepwater CO_2 between the last glaciation and the Holocene. *Paleoceanogr.* **3**: 317–341.

DUPLESSY, J. C.; N. J. SHACKLETON, R. G. FAIRBANKS, L. LABEYRIE, D. OPPO and N. KALLEL. 1988. Deep water source variations during the last climatic cycle and their impact on the global deepwater circulation. *Paleoceanogr.* **3**: 343–360.

FAIRBANKS, R. G. 1989. A 17000-year glacio-eustatic sea level record: influence of glacial melting rates on the Younger Dryas event and deep-ocean circulation. *Nature*, **342**: 637–642.

FLATO, G. M. and W. D. HIBLER III. 1992. Modelling pack ice as a cavitating fluid. *J. Phys. Oceanogr.* **22**: 626–651.

FLATO, G. M. and G. J. BOER. 2001. Warming asymmetry in climate change simulations. *Geophys. Res. Lett.* **28**: 195–198.

FREELAND, H. J.; A. S. BYCHKOV, F. WHITNEY, C. TAYLOR, C. S. WONG and G. I. YURASOV. 1998. WOCE section P1W in the Sea of Okhotsk 1. Oceanographic data description. *J. Geophys. Res.* **103**: 15613–15615.

GENT, P. R. and J. C. MCWILLIAMS. 1990. Isopycnal mixing in ocean circulation models. *J. Phys. Ocenaogr.* **20**: 150–155.

GLADYSHEV, S.; S. MARTIN, S. RISER and A. FIGURKIN. 2000. Dense water production on the northern Okhotsk shelves: Comparison of ship-based spring-summer observations for 1996 and 1997 with satellite observations. *J. Geophys. Res.* **105**: 26281–26299.

GORBARENKO, S. A. 1996. Stable isotope and lothologic evidence of Late-Glacial and Holocene oceanography of the Northwestern Pacific and its marginal seas. *Quat. Res.* **46**: 230–250.

HEWITT, C. D. and J. F. MITCHELL. 1997. Radiative forcing and response of a GCM to ice age boundary conditions: cloud feedback and climate sensitivity. *Clim. Dyn.* **13**: 821–834.

HEWITT, C. D.; A. C. BROCCOLI, J. F. MITCHELL and R. J. STOUFFER. 2001. A coupled model study of the last glacial maximum: Was part of the North Atlantic relatively warm? *Geophys. Res. Lett.* **28**: 1571–1574.

IKEHARA, K. 2003. Late Quaternary seasonal sea-ice history of the Northeastern Japan Sea. *J. Oceanogr.* **59**: 585–593.

KAGEYAMA, M.; A. LAÎNÉ, A. ABE-OUCHI, P. BRACONNOT, E. CORTIJO, M. CRUCIFIX, A. DE VERNAL, J. GUIOT, C. D. HEWITT, A. KITOH, M. KUCERA, O. MARTI, R. OHGAITO, B. OTTO-BLIESNER, W. R. PELTIER, A. ROSELL-MELÉ, G. VETTORETTI, S. L. WEBER, Y. YU and MARGO PROJECT MEMBERS. 2006. Last Glacial Maximum temperatures over the North Atlantic, Europe and western Siberia: a comparison between PMIP models, MARGO sea–surface temperatures and pollen-based reconstructions. *Quat. Sci. Rev.* **25**: 2082–2102.

KEIGWIN, L. D. 1998. Glacial-age hydrography of the far northwest Pacific Ocean. *Paleoceanogr.* **13**(4): 323–339.

KENT, D.; N. D. OPDYKE and M. EWING. 1971. Climate changes in the North Pacific using ice-rafted detritus as a climate indicator. *Geol. Soc. Am. Bull.* **82**: 2741–2754.

KILLWORTH, P. D. 1983. Deep convection in the world ocean. *Rev. Geophys.* **21**: 1–26.

KIM, S.-J. 2004a. The effect of atmospheric CO_2 and ice sheet topography on LGM climate. *Clim. Dyn.* **22**: 639–651.

KIM, S.-J. 2004b. A coupled model simulation of ocean thermohaline properties of the Last Glacial Maximum. ATMOSPHERE-OCEAN, **42**(3): 213–220.

KIM, S.-J.; G. M. FLATO, G. J. BOER and N. A. MCFARLANE. 2002. A coupled climate model simulation of the Last Glacial Maximum, Part 1: transient multi-decadal response. *Clim. Dyn*. **19**: 515–537.

KIM, S.-J.; G. M. FLATO and G. J. BOER. 2003. A coupled climate model simulation of the Last Glacial Maximum, Part 2: approach to equilibrium. *Clim. Dyn.* **20**: 635–661.

KITANI, K. 1973. An oceanographic study of the Okhotsk Sea - particularly in respect to cold waters. *Bull. Far Seas Fish. Res. Lab.* **9**: 45–76.

KITOH, A.; S. MURAKAMI and H. KOIDE. 2001. A simulation of the Last Glacial Maximum with a coupled atmosphere-ocean GCM. *Geophys. Res. Lett.* **28**: 2221–2224.

KOBAYASHI, T. 1999. Study of the formation of North Pacific Intermediate Water by a general circulation model and the particle-tracking method 1. A pitfall of general circulation model studies. *J. Geophys. Res.* **104**: 5423–5439.

LEE, K. E. and Y.-G. PARK. 2003. Seasonal changes in sea surface temperature of the subtropical North Pacific during the last glaciation. *Geosci. J*. **7**: 129–133.

LEVITUS, S. and T. P. BOYER. 1994. World ocean atlas 1994 Vol. 4: temperature. NOAA Atlas NESIDIS 4, US Department of Commerce, 117 pp.

LEVITUS, S.; R. BURGETT and T. P. BOYER. 1994. World ocean atlas 1994 Vol. 3: salinity. NOAA Atlas NESIDIS 3, US Department of Commerce, 99 pp.

MACDONALD, A. M. 1998. The global ocean circulation: a hydrographic estimate and regional analysis. *Progr. Oceanogr.* **41**: 281–382.

MARTIN, S.; R. DRUCKER and K. YAMASHITA. 1998. The production of ice and dense shelf water in the Okhotsk Sea polynyas. *J. Geophys. Res.* **103**: 27771–27782.

MCCARTNEY, M. S. 1977. Subantarctic Mode Water. In: *A Voyage of Discovery: George Deacon 70th Anniversary Volume*. M. V. Angel (Eds.), Supplement to Deep-Sea Research, Pergamon Press, Oxford, pp. 103–119.

MCFARLANE, N. A.; G. J. BOER, J.-P. BLANCHET and M. LAZARE. 1992. The Canadian Climate Centre Second-Generation General Circulation Model and its equilibrium climate. *J. Clim.* **5**: 1013–1044.

MOLINELLI, E. 1978. Isohaline thermoclines in the southeast Pacific Ocean. *J. Phys. Oceanogr.* **8**: 1139–1145.

MORIMOTO, A. and T. YANAGI. 2001. Variability of sea surface circulation in the Japan Sea. *J. Oceanogr.* **57**: 1–13.

OKOUCHI, N.; H. KAWAHATA, M. MURAYAMA, M. OKADA, T. NAKAMURA and A. TAIRA. 1994. Was deep water formed in the North Pacific during the Late Quaternary? Cadmium evidence from the northwest Pacific. *Earth Planet. Sci. Lett.* **124**: 185–194.

OPPO, D. W. and R. G. FAIRBANKS. 1987. Variability in the deep and intermediate water circulation of the Atlantic Ocean during the past 25,000 years: Northern Hemisphere modulation of the Southern Ocean. *Earth Planet. Sci. Lett.* **86**: 1–15.

PACANOWSKI, R. C.; K. DIXON and A. ROSATI. 1993. The GFDL modular ocean model users guide. GFDL Ocean Group Tech Rep 2. Geophysical Fluid Dynamics Laboratory, Princeton, USA, 46 pp.

PELTIER, W. R. 1994. Ice age paleotopography. *Science,* **265**: 195–201.

PELTIER, W. R. and L. P. SOLHEIM. 2004. The climate of the Earth at the Last Glacial Maximum: statistical equilibrium state and a mode of internal variability. *Quat. Sci. Rev.* **23**: 335–357.

PETIT, J. R.; J. JOUZEL, D. RAYNAUD, N. I. BARKOV, J.-M. BARNOLA, I. BASILE, M. BENDER, J. CHAPPELLAZ, M. DAVIS, G. DELAYGUE, M. DELMOTTE, V. M. KOTLYAKOV, M. LEGRAND, V. Y. LIPENKOV, C. LORIUS, L. PEPIN, C. RITZ, E. SALTZMAN and M. STIEVENARD. 1999. Climate and atmospheric history of the past 420,000 years from the Vostok ice core, Antarctica. *Nature*, **399**: 429–436.

REID, J. 1965. Intermediate waters of the Pacific Ocean. Johns Hopkins Oceanography Studies, No. 2, 85 pp.

SAENKO, O. A.; A. SCHMITTNER and A. J. WEAVER. 2004. The Atlantic-Pacific Seesaw. *J. Clim.* **17**(11): 2033–2038.

SAWADA, K. and N. HANDA. 1998. Variability of the path of the Kuroshio ocean current over the past 25,000 years. *Nature,* **392**: 592–595.

SCHMID, C.; G. SIEDLER and W. ZENK. 2000. Dynamics of Intermediate Water Circulation in the subtropical South Atlantic. *J. Phys. Oceanogr.* **30**: 3191–3211.

SEIDOV, D.; B. J. HAUPT, E. J. BARRON and M. MASLIN. 2001. Ocean bi-polar seesaw and climate : Southern versus northern melt water impacts. In: *The Oceans and Rapid Climate Change, Past, Present, and Future*. D. Seidov, B. Haupt, and M. Maslin (Eds), Geophysical Monograph, Vol. 126, Am. Geophys. Union, pp. 147–167.

SEIDOV, D. and B. J. HAUPT. 2003. Freshwater teleconnections and ocean thermohaline circulation. *Geophys. Res. Lett.* **30**: doi:10.1029/2002GL016564.

SEMTNER, A. J. 1976. A model for thermodynamic growth of sea ice in numerical investigations of climate. *J. Phys. Oceanogr.* **6**: 379–389.

SHCHERBINA, A. Y.; L. D. TALLEY and D. L. RUDNICK. 2003. Direct observations of North Pacific ventilation: Brine rejection in the Okhotsk Sea. *Science*, **302**: 1952–1955.

SHIN, S.-I.; Z. LIU, B. OTTO-BLIESNER, E. BRADY, J. KUTZBACH and S. HARRISON. 2003. A simulation of the Last Glacial Maximum climate using the NCAR-CCSM. *Clim. Dyn*. **20**: 127–151.

SØRENSEN, J. V. T.; J. RIBBE and G. SHAFFER. 2001. Antarctic Intermediate Water mass formation in ocean general circulation models. *J. Phys. Oceanogr.* **31**: 3295–3311.

SVERDRUP, H. U.; M. W. JOHNSON and R. H. FLEMING. 1942. *The oceans: Their physics, chemistry and general biology.* Prentice-Hall, Englewood Cliffs, New York, 1087 pp.

TALLEY, L. D. 1985. Ventilation of the subtropical North Pacific: the shallow salinity minimum. *J. Phys. Oceanogr.* **15**: 633–649.

TALLEY, L. D. 1991. An Okhotsk Sea anomaly: Implications for ventilation in the North Pacific. *Deep Sea Res.* **38**: S171–S190.

TALLEY, L. D. 1993. Distribution and formation of North Pacific Intermediate Water. *J. Phys. Oceanogr.* **23**: 517–537.

TALLEY, L. D. 1997. North Pacific intermediate water transports in the mixed water region. *J. Phys. Oceanogr.* **27**: 1795–1803.

TALLEY, L. D. 2003. Shallow, intermediate, and deep overturning components of the global heat budget. *J. Phys. Oceanogr.* **33**: 530–560.

TALLEY, L. D. and M. S. MCCARTNEY. 1982. Distribution and circulation of Labrador Sea Water. *J. Phys. Oceanogr.* **12**: 1189–1205.

TALLEY, L. D.; Y. NAGATA, M. FUJIMURA, T. KONO, D. INAGAKE, M. HIRAI and K. OKUDA. 1995. North Pacific Intermediate Water in the Kuroshio/Oyashio mixed water region. *J. Phys. Oceanogr.* **25**: 475–501.

TANIMURA, Y. 1999. Varieties of a single cosmopolitan diatom species associated with surface water masses in the North Pacific. *Marine Micropaleontol.* **37**: 199–218.

WARREN, B. A. 1981. Deep circulation of the world ocean. In: *Evolution of Physical Oceanography*, B. A. Warren and C. Wunsch (Eds), The MIT Press, pp. 6–41.

WARREN, B. A. 1983. Why is no deep water formed in the North Pacific? *J. Marine Res.* **41**: 327-347.

WATANABE, T. and M. WAKATSUCHI. 1998. Formation of 26.8-26.9 σ_θ water in the Kuril Basin of the Sea of Okhotsk as a possible origin of North Pacific Intermediate Water. *J. Geophys. Res.* **103**: 2849–2865.

WYPUTTA, U. and B. J. MCAVANEY. 2001. Influence of vegetation changes during the Last Glacial Maximum using the BMRC atmospheric general circulation model. *Clim. Dyn.* **17**: 923–932.

YANASE, W. and A. ABE-OUCHI. 2007. The LGM surface climate and atmospheric circulation over east Asia and the north Pacific in the PMIP2 coupled model simulations. *Clim. Past*. **3**: 439–451.

YASUDA, I. 1997. The origin of the North Pacific Intermediate Water. *J. Geophys. Res.* **102**: 893–909.

YASUDA, I.; K. OKUDA and Y. SHIMIZU. 1996. Distribution and modification of North Pacific Intermediate Water in the Kuroshio-Oyashio Interfrontal Zone. *J. Phys. Oceanogr.* **26**: 448–465.

YOKOYAMA, Y.; K. LAMBECK, P. DE DECKKER, P. JOHNSTON and L. K. FIFIELD. 2000. Timing of the Last Glacial Maximum from observed sea-level minima. *Nature*, **406**: 713–716.

YUAN, X. and L. D. TALLEY. 1996. The subarctic frontal zone in the North Pacific: Characteristics of frontal structure from climatological data and synoptic surveys. *J. Geophys. Res.* **101**: 16491–16508.